

3D Printing of Liquid Crystal Elastomeric Actuators with Spatially Programmed Nematic Order

Arda Kotikian, Ryan L. Truby, John William Boley, Timothy J. White, and Jennifer A. Lewis*

Liquid crystal elastomers (LCEs) are soft materials capable of large, reversible shape changes, which may find potential application as artificial muscles, soft robots, and dynamic functional architectures. Here, the design and additive manufacturing of LCE actuators (LCEAs) with spatially programmed nematic order that exhibit large, reversible, and repeatable contraction with high specific work capacity are reported. First, a photopolymerizable, solvent-free, main-chain LCE ink is created via aza-Michael addition with the appropriate viscoelastic properties for 3D printing. Next, high operating temperature direct ink writing of LCE inks is used to align their mesogen domains along the direction of the print path. To demonstrate the power of this additive manufacturing approach, shape-morphing LCEA architectures are fabricated, which undergo reversible planar-to-3D and 3D-to-3D' transformations on demand, that can lift significantly more weight than other LCEAs reported to date.

Liquid crystal elastomers (LCEs) are soft materials capable of large, reversible shape changes, which may find potential application as artificial muscles,^[1,2] soft robots,^[3,4] and dynamic functional architectures.^[5–9] Two important approaches have emerged for synthesizing LCEs; one involves the incorporation of mesogens as side chains in siloxane elastomers,^[10] while the other integrates mesogens within the main chains via chain-extending reactions.^[11] Both types of LCEs undergo a large contraction along the direction of the nematic director, i.e., parallel to the direction of mesogen alignment, when heated above their nematic-isotropic temperature (T_{NI}),^[10–12] swelled by solvent^[11,13] or exposed to light to induce *cis-trans* conformational changes in the case of light-responsive mesogens.^[14,15]

To date, the alignment of LCEs has been primarily achieved in thin films (thickness < 100 μm) via molecular interactions with command surfaces,^[12–15] mechanical stretching,^[10,16,17] or

applied magnetic fields.^[18–20] Although thicker LCEs can be produced with the latter approaches, they typically possess uniaxially aligned directors. Recently, both LCE thin films^[11] and 3D structures^[21] have been fabricated with programmable control over their director orientation. Using an optical patterning system, White and co-workers^[11] created voxelated command surfaces composed of azobenzene-based photoalignment materials, whose orientation is defined with high spatial precision (minimum area $\approx 0.01 \text{ mm}^2$) through control of the electric field vector of the linearly polarized light. Using a two-step synthesis method, they produced LCEs composed of a poly(b-amino ester) network. First, low viscosity precursors are aligned on the patterned command surface, and then the monomers undergo

chain extension reactions to form main-chain nematic macromers that are subsequently cross-linked. Their voxelated LCE thin films exhibit large shape changes and specific work. Quite recently, Ware and co-workers designed a LCE ink based on this chemistry and reported the 4D printing of shape-morphing LCE architectures in both planar and 3D motifs, including those with opposing negative and positive Gaussian curvatures that exhibit reversible snap-through transitions.^[21]

Here, we report the design and additive manufacturing of LCE actuators (LCEAs) with spatially programmed nematic order in arbitrary form factors. Unlike soft actuators based on shape memory polymers, elastomeric matrices with embedded pneumatic channels, or electroactive polymers that require mechanical preprogramming, external pressure sources,^[22] or large voltages,^[23] respectively, LCEAs exhibit large, reversible, and repeatable contraction with high specific work capacity.^[24,25] We use high operating temperature direct ink writing (HOT-DIW)^[26] of LCE inks to align their mesogen domains along the direction of the print path (**Figure 1**). We then characterize their order parameter, actuation strain, and specific work. Using this process, we create shape-morphing LCEA architectures that undergo reversible planar-to-3D and 3D-to-3D' transformations on demand as well as 3D LCEAs ($\approx 1 \text{ mm}$ thick) capable of lifting 233% more weight than other LCEAs reported to date.^[27]

The alignment of liquid crystalline domains during HOT-DIW is dependent on the LCE ink composition, rheology, and printing parameters. To maximize their potential actuation strain, we designed a photopolymerizable, solvent-free, main-chain LCE ink.^[11] Specifically, this ink is produced by creating oligomers from a reactive mesogen and amine linker

A. Kotikian, Dr. R. L. Truby, Dr. J. W. Boley, Prof. J. A. Lewis
John A. Paulson School of Engineering and Applied Sciences
and Wyss Institute for Biologically Inspired Engineering
Harvard University
Cambridge, MA 02138, USA
E-mail: jalewis@seas.harvard.edu

Dr. T. J. White
Air Force Research Laboratory
Materials and Manufacturing Directorate
Wright-Patterson Air Force Base
OH 45433, USA

 The ORCID identification number(s) for the author(s) of this article can be found under <https://doi.org/10.1002/adma.201706164>.

DOI: 10.1002/adma.201706164

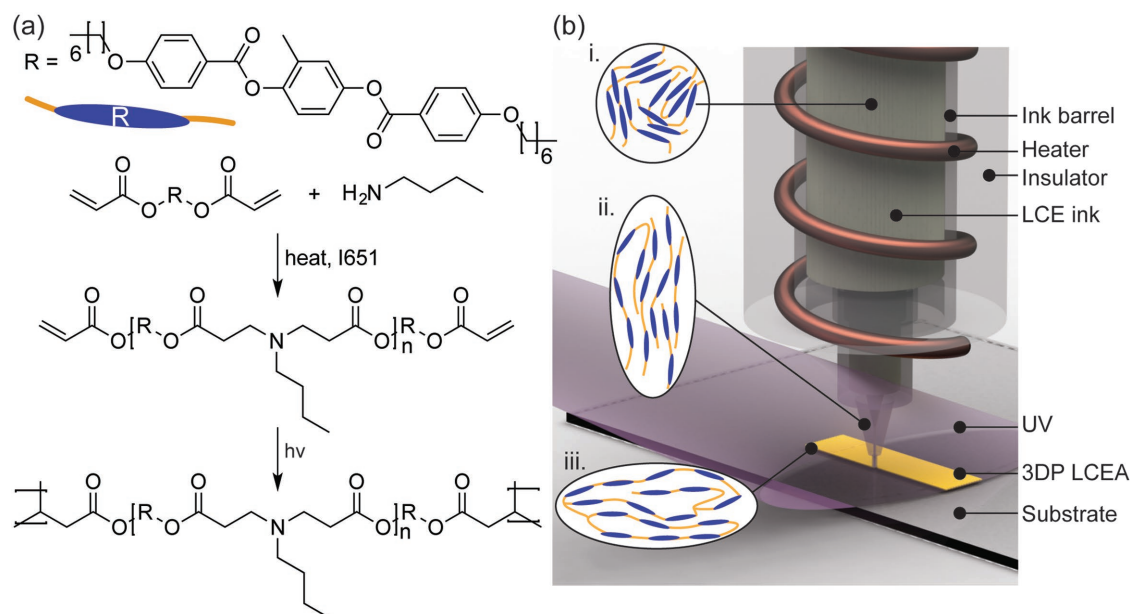


Figure 1. LCE ink design and printing. a) One-pot synthesis of the photopolymerizable LCE ink that includes a spacer (yellow chain), mesogen (R), and photoinitiator. b) Schematic illustration of HOT-DIW of the LCE ink, where (i) shows the disordered LCE ink morphology inside the heated barrel, (ii) ordered morphology that emerges due to induced director alignment within the nozzle, and (iii) resulting ordered morphology in printed and crosslinked LCE filaments.

via aza-Michael addition (Figure 1a).^[11,12] Reactive acrylate end groups ensure that the 3D printed LCEAs form crosslinks upon UV exposure, which is essential for retaining the programmed mesogen alignment imposed by the printing process. Solvent-free LCE inks not only enable elongation of liquid crystal polymer chains at lower shear rates and molecular weight than their solvent-based counterparts,^[28] they avoid the volumetric changes and residual stresses that arise from solvent loss during drying.

We printed the LCE ink at elevated temperatures between T_g and T_{NI} using HOT-DIW (Figures 1b; Figure S1 and Movie S1, Supporting Information), i.e., between -22 and 95 °C, respectively, as determined by differential scanning calorimetry (Figure S2a, Supporting Information). This large temperature range provides a broad window for 3D printing LCEAs with programmed director alignment.^[29] As temperature is increased in the nematic state, the LCE viscosity decreases dramatically from 25 to 80 °C and concomitantly, it becomes less shear thinning. In the isotropic state (120 °C), the LCE ink is a Newtonian fluid with a viscosity that is roughly two orders of magnitude lower than the value measured at room temperature (Figure S2b, Supporting Information). To enable HOT-DIW printing of high fidelity architectures, the LCE ink must possess a strong shear thinning response. We therefore selected a printing temperature of 50 °C, where the LCE ink also exhibits a viscoelastic response that facilitates its shape retention during the printing process (Figure S2c, Supporting Information). The as-printed LCE features are exposed to UV light to induce cross-links between reactive end groups, which preserve the programmed director alignment within the printed LCEA architectures.

To demonstrate spatial control over director alignment during HOT-DIW, we first printed an LCEA bilayer composed of an H-shaped layer (top, 100 μm thick) and a square-shaped

layer (bottom, 100 μm thick, 12 mm \times 12 mm wide) patterned on a glass substrate using a nozzle diameter of 250 μm and a print speed of 4 mm s^{-1} at 50 °C (Figure 2a). The H-shaped layer consists of an array of LCE filaments printed in a meanderline pattern using a 90° (from horizontal) print path, while the square layer is printed using a diagonal (45° from horizontal) print path. Using polarized optical microscopy, one clearly observes the spatial control of the director along the direction of print path, i.e., only the H-shaped layer is bright when the cross-polarizers are oriented at $45^\circ/135^\circ$ (Figure 2a, top), while only the square layer is bright (Figure 2a, bottom) when they are oriented at $0^\circ/90^\circ$. To determine the effect of temperature on director alignment, we printed samples (125 μm height) both below (50 °C) and above (105 °C) T_{NI} using a 250 μm nozzle and printing speeds between 2 and 10 mm s^{-1} . Note, different applied pressures are used to ensure that the printed filament width (100 μm width \times 125 μm height) is approximately the same in all cases. LCE samples printed at 50 °C had better director alignment along the print path, i.e., a higher order parameter (Figure 2b; see also Figure S3, Supporting Information) than samples printed at 105 °C. The LCE ink is subjected to both shear and extensional flow during the HOT-DIW process,^[30] which induces alignment of their mesogenic domains.^[29,31] As expected, the order parameter of LCEA samples printed at 50 °C increases with print speed due to enhanced director alignment (Figure 2c; see also Table S1, Supporting Information).

To investigate their actuation performance, we printed LCEA bilayers ($15 \times 3 \times 0.25$ mm) using a nozzle diameter of 250 μm , average print speed of 4.8 mm s^{-1} and a meanderline horizontal print path. The printed LCEA bilayers are then cycled 20 times between ≈ 26 and 105 °C (Figure 3a; Movie S2, Supporting Information). For these experimental conditions,

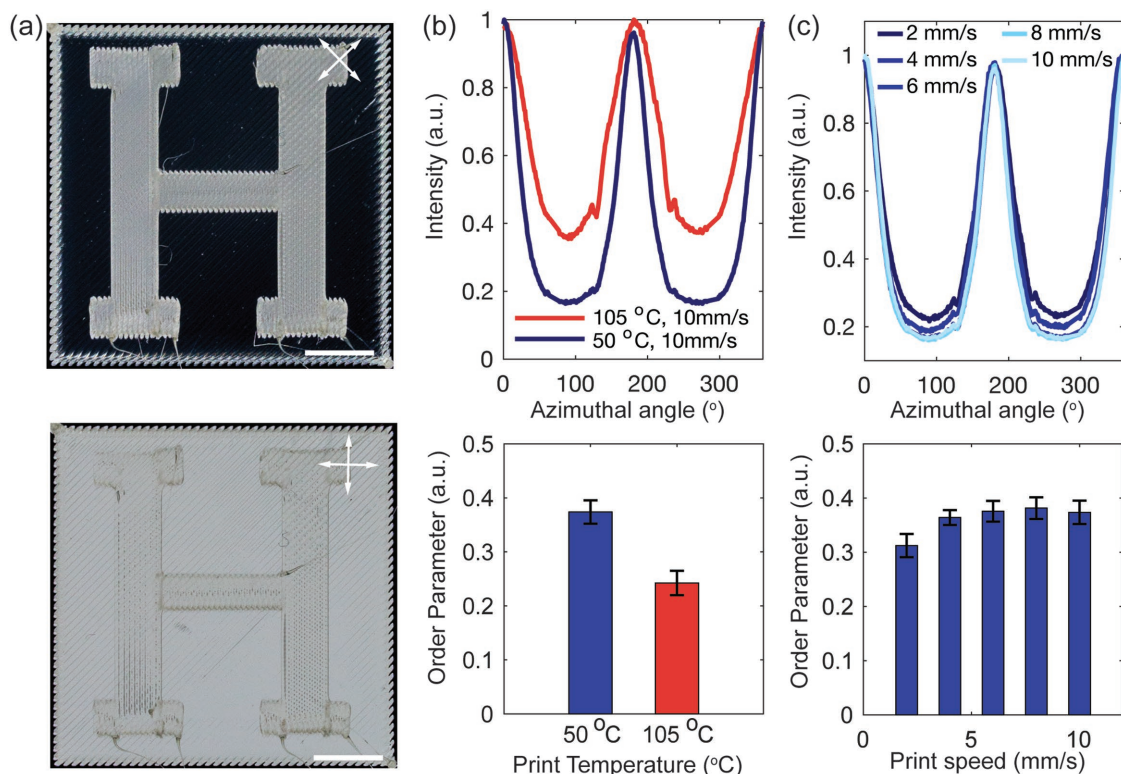


Figure 2. Spatial programming of the director. a) Polarized optical microscopy (POM) images of a printed LCE structure composed of an underlying square layer printed using a diagonal meander and a top layer composed of an orthogonally printed “H”-shape taken using rotated polarizers (scale bar = 2.5 mm). b) Plot of intensity as a function azimuthal angle for LCE samples printed at 50 and 105 °C at 10 mm s⁻¹ (top) and their corresponding order parameters (bottom). c) Plot of intensity as a function of azimuthal angle of LCE samples printed at 50 °C at varying speed (top) and their corresponding order parameters (bottom).

we measured an average repeatable actuation contraction of $-43.6 \pm 6.7\%$ along the print direction and an average expansion of $29.8 \pm 5.9\%$ normal to that direction (Figure 3b). We note that these LCEAs can be successfully cycled up to 100 times (Figure S4, Supporting Information). Full actuation of these printed LCEA occurs in ≈ 180 s, while relaxation back to their original dimensions requires 210 s (Figure S5, Supporting Information). Hence, a conservative estimate of the cycle time required to “reversibly switch” these printed LCEAs is ≈ 390 s for the thermal cycling conditions used. We note that longer cooling times are needed due to the lack of active cooling. Next, we printed LCEAs (1 mm thick) using a nozzle diameter of 250 μm , average print speed of 3.7 mm s⁻¹, and a meanderline print path and explored their ability to contract when tethered to different weights (Figure 3c; Movie S3, Supporting Information). In these weight-lifting experiments, strain is calculated using the unloaded LCEA length (Figure 3c, left) as the initial length, rather than the elongated length when loaded (Figure 3c, middle) below T_{NI} , and its final length after the loaded LCEA is heated above T_{NI} (Figure 3c, right). Importantly, these thick LCEAs can lift roughly 1000 times their own weight of 106 ± 1.5 mg. With increased weight loading, the actuation strain for the LCEAs decreases and the actuator work increases, with a maximum energy density of 39 J kg⁻¹ (Figure 3d). Since they are not composed of a single domain, the LCEAs can elongate upon heating to a more ordered state^[32,33] prior to

contraction (Movie S3, Supporting Information). If the contraction does not surpass the original length, the actuation strain is noted as a positive value and negative work (Figure 3d). Upon cooling, the LCEAs return to within 11% of their initial length. To impart larger contractile strains at an even larger bias stress, one can simply print thicker actuators. Based on the stress–strain measurements reported in Figure S6 (Supporting Information), these printed LCEAs exhibit an elastic modulus of 3.1 ± 0.3 MPa at room temperature when loaded along the print direction.

As a final demonstration, we printed LCEAs with spatially programmed directors that are capable of complex, reversible shape transformations. First, to program shape change into a cone with positive Gaussian curvature, LCEAs (of diameter 10 mm) are printed using a nozzle diameter of 250 μm and print speed of 4.5 mm s⁻¹ with four layers (0.4 mm thick) each of which is based on equivalent Archimedean spiral print paths (Figure 4a; Movie S4, Supporting Information). Using this type of print path,^[34] the LCEA transforms into a cone with a maximum height of 6.5 mm when heated above T_{NI} , which corresponds to a 1628% stroke out-of-plane. As expected, the LCEA recovers its original dimensions and shape upon cooling (Figure S7a, Supporting Information). We also printed LCEAs capable of morphing into shapes with negative Gaussian curvature with 5 mm s⁻¹ print speed (Figure 4b; Movie S5, Supporting Information). In these four-layer LCEAs (0.4 mm thick),

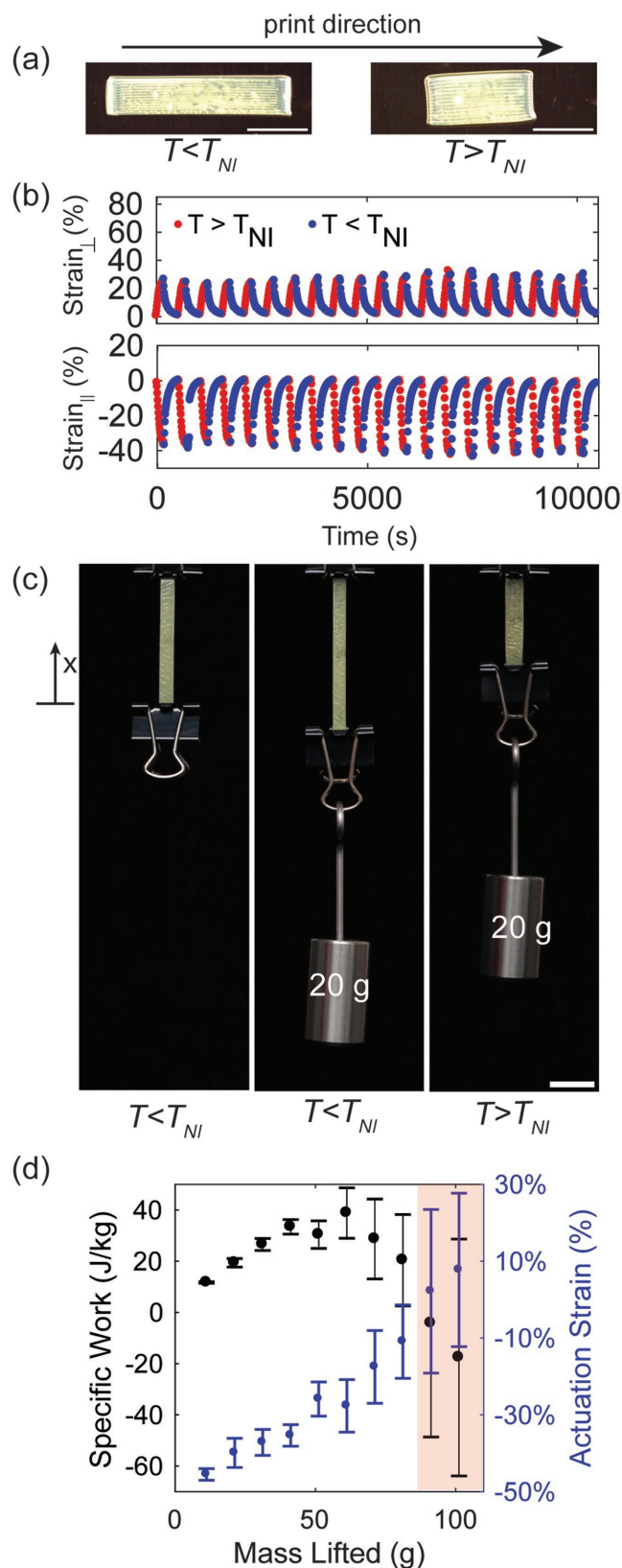


Figure 3. Printed LCE Actuators. a) Images of printed (left) and actuated (right) LCEAs fabricated using a unidirectional print path (scale bar = 5 mm). b) Their measured strain in the direction perpendicular and parallel to the print path upon cycling the LCEAs above and below

the top and bottom pairs of layers are printed using perpendicularly oriented, in-filled meanders. Upon heating, this LCEA morphs into a saddle form.^[34] However, due to residual stresses introduced during inline UV crosslinking, it does not return to its original flat conformation upon cooling, but rather snaps into an inverted saddle configuration (Figure S7b and Movie S6, Supporting Information). When heated again, it snaps back into the programmed saddle configuration, and alternating actuation between both configurations is observed upon thermal cycling. Hence, after the initial actuation, this LCEA exhibits a repeatable 3D-to-3D' shape transformation. Next, we created in-plane mechanical metamaterials in the form of printed LCEA meshes with an inner strut width of 0.86 mm and thickness of 0.5 mm (Figure 4c; Movie S7, Supporting Information), which shrinks isotropically $\approx 18\%$ in-plane (i.e., both horizontally and vertically) and recovers to their initial dimensions upon cooling to room temperature (Figure S7c, Supporting Information). Lastly, we printed a larger LCEA ($2.5 \times 2.5 \text{ cm}^2$) capable of out-of-plane shape change (Figure 4d; Movies S8 and S9, Supporting Information) using a print path that consists of a square spiral array (see Figure S8, Supporting Information, which shows the resulting director alignment). This LCEA morphs out-of-plane into an array of cones with a maximum height of 1.92 mm upon heating to $95 \text{ }^\circ\text{C}$, returning to its near-initial conformation upon cooling (Figure S7d, Supporting Information).

In summary, we have demonstrated the ability to create LCEAs with programmed director alignment by HOT-DIW. By controlling the ink composition, rheology, and printing parameters, LCEAs were fabricated in multilayered structures with arbitrary thickness and overall dimensions. These LCEAs exhibited large contractions when heated to temperatures above their nematic-to-isotropic phase transition, which enabled their exceptional actuation performance with a maximum energy density of 39 J kg^{-1} , actuation of up to 70 g loads, and complex shape-morphing capabilities, including both 2D-to-3D and 3D-to-3D' transformations. Additive manufacturing of LCEA architectures opens new avenues for creating artificial muscles, soft robotics, and other dynamic functional structures based on these materials.

Experimental Section

LCE Ink: The LCE ink was prepared by a modified one-pot synthesis reported previously^[12] utilizing a catalyst-free aza-Michael addition chemistry. As-received 1,4-Bis-[4-(6-acryloyloxyhexyloxy)benzoyloxy]-2-methylbenzene (Synthon, 97%, 2 g), n-butylamine (Sigma-Aldrich, 99.5%), and Irgacure 651 (I651, BASF) were added to a 25 mL round bottom flask in 1:1 molar ratio and 2 wt%, respectively. The mixture was heated to $110 \text{ }^\circ\text{C}$, above the melting point of the mesogen and the T_{NI} of the resulting LCE, and stirred vigorously. The reaction was shielded from fluorescent light, and the clear, yellow product was quenched in ice after 18 h.

3D Printing: The HOT-DIW setup was a modification on a previously demonstrated custom print setup (Figure S1, Supporting Information).^[26] Briefly, it was comprised of a steel barrel surrounded

T_{NI} . c) Image sequence obtained for a LCEA (1 mm thick) printed using a unidirectional print path lifting a 20 g weight, which shows the LCEA in the unloaded (left) and loaded states with the 20 g weight (middle) at $T < T_{NI}$, and the actuated state when $T > T_{NI}$ (right) (scale bar = 10 mm). d) Specific work (work normalized by actuator mass) and actuation strain of LCEAs lifting different weights. Red highlights the weight range over which the average LCEA does not contract in positive (x) direction.

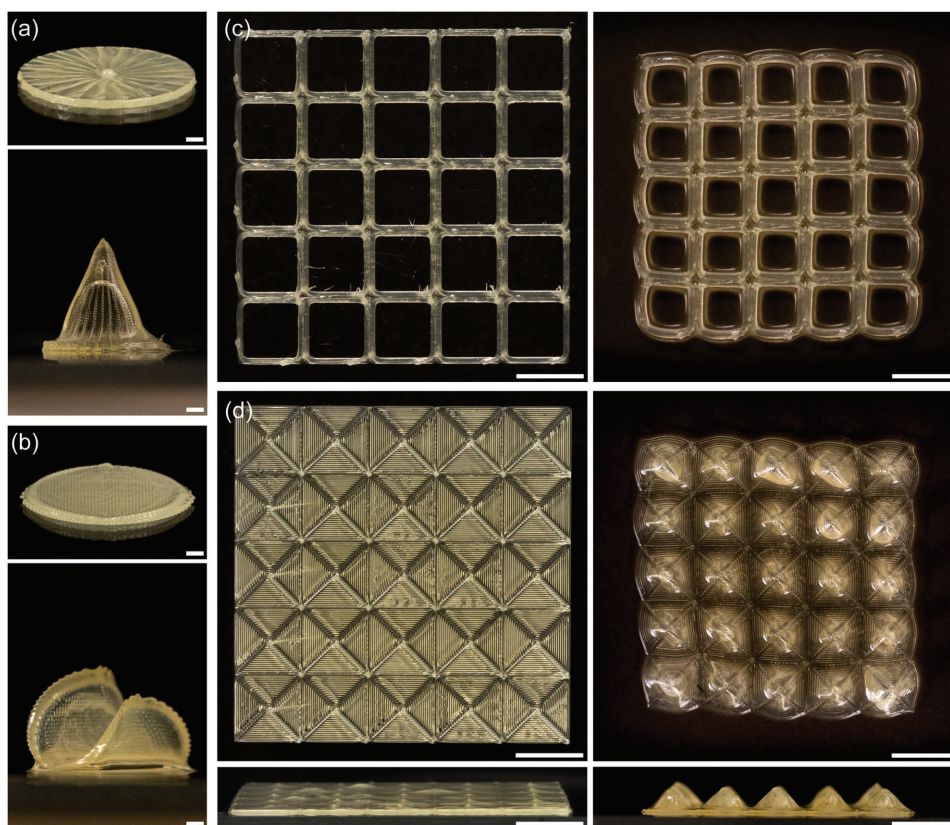


Figure 4. Programmable shape morphing LCEAs. a,b) Images of disc-shaped LCEAs (≈ 0.4 mm thick) printed using layered spiral (a, top) and layered perpendicular meanders (b, top) print paths (scale bars = 1 mm). Upon heating above T_{NI} , these LCEAs morph into a cone (a, bottom) and saddle (b, bottom) shape, respectively (scale bars are 1 mm). c) Top-down images of mesh-shaped LCEAs (≈ 0.5 mm thick) after printing (left) and shrinking into an isotropic form (right) upon heating above T_{NI} (scale bars = 5 mm). d) Top view (upper row) and side view (lower row) of a LCEA sheet after printing (left) and morphing (right) into a conical array upon heating above T_{NI} (scale bars = 5 mm).

by a heater coil (FM Keefe Company Inc., 62H36A5X-1128) with temperature readout by thermocouple (k-type) at the tip of the stainless steel nozzle (TecDia Inc., ARQ-S-2535) and internal temperature readout by thermocouple (K-type) to prevent heating the barrel above the T_{NI} while printing. The temperature of the nozzle was set to the print temperature of 50 °C and maintained with a temperature controller (Omega, CNI16). HOT-DIW was performed with a custom three-axis motion control stage (Aerotech Inc.) that deposits ink via pressure-driven extrusion with an Ultimix V pressure box (Nordson EFD) according to programmed G-code (Mecode). LCEAs were printed on precleaned glass substrates secured to a leveled multiaxis stage (ThorLabs). Each batch of ink (≈ 2 g) was manually consolidated into large pellets and loaded into the barrel at room temperature. The temperature was increased above T_{NI} , then cooled at ≈ 10 °C min^{-1} rate until the nozzle temperature reached that of the prescribed printing temperature. The system was held at this temperature (typically 50 °C) for ≈ 30 min prior to printing to allow the system to reach a steady state operating condition. As the ink was extruded, it was exposed to UV light (Omnicure, S2000) at an intensity of ≈ 12 mW cm^{-2} (Figure S1, Supporting Information). After printing, LCEAs were exposed to higher intensity UV (≈ 31 mW cm^{-2}) for 20 min (10 min for the top and bottom sides) to ensure uniform crosslinking. Printed LCEAs that were thicker than two filamentary layers were exposed to UV light every two layers for 400 s (≈ 31 mW cm^{-2}).

Differential Scanning Calorimetry: The LCE ink was heated to 120 °C to erase any thermal history, cooled to -50 °C, then heated to 200 °C, all at a rate of 10 °C min^{-1} (Q200; TA Instruments).

Ink Rheology: The rheological properties of the LCE ink were characterized using a controlled stress rheometer (Discovery HR-3 Hybrid Rheometer; TA Instruments) equipped with 20 mm steel Peltier

plate geometry and 0.750 mm gap. Prior to testing, the ink was brought to T_{NI} to erase the thermal history.

Wide Angle X-ray Scattering (WAXS): X-ray measurements were performed on a SAXSLAB system with a Rigaku 002 microfocus X-ray source ($\text{CuK}_{\alpha 1} = 1.5409$ Å) with sample to detector (PILATUS 300K, Dectris) distance of 109.1 mm for 15 min with Osmic staggered parabolic multilayer optics to focus the beam crossover at the second pinhole. It contains two sets of JJ X-ray 4 jaw collimation slits that are 0.9 mm. WAXS samples consisted of one-layer LCEAs printed as unidirectional strips. Their order parameter was calculated from the WAXS data using Equation (1) by numerically integrating (MATLAB function trapz)

$$S = \bar{P}_2 = 1 - N^{-1} \frac{3}{2} \int_0^{\pi/2} I(\theta) \left[\sin^2 \theta + (\sin \theta \cos^2 \theta) \log \frac{1 + \sin \theta}{\cos \theta} \right] d\theta \quad (1)$$

where $N = \int_0^{\pi/2} I(\theta) d\theta$.^[35]

Imaging and Image Analysis: Printed LCE architectures were photographed using a camera (Canon 5D Mark III) between crossed polarizers (ThorLabs) keeping imaging conditions constant for both positions of crossed polarizers. Micrographs of unidirectional LCE samples were obtained using an inverted microscope equipped with crossed polarizers (Axio Observer, Zeiss).

Actuation Measurements: Cyclic actuation measurements were performed on a custom three-axis motion control stage. Printed LCEAs were placed on a thin silicone oil layer on top of an anodized aluminum stage and lowered onto and raised off of a hotplate such that their temperature was alternated between room temperature (held for 210 s)

and 105 °C (for 180 s), respectively (Figure S5, Supporting Information). Photographs of these LCEA samples were taken throughout this process (Canon EOS 5D Mark III) at a frequency of 0.1 Hz. An in-house MATLAB image analysis script was used to determine the dimensions of the actuated samples. To demonstrate their ability to lift weight, mass standards (Spectrum Chemicals) were attached to printed LCEAs with a binder clip (1.19 g) and heated with a heat gun (Milwaukee, MHT3300). To demonstrate their ability to reversibly change shape, printed LCEAs were heated using a hot plate (IKA RET basic) and imaged during this process. The saddle LCEA was actuated on a hot plate held at 90 °C, while the spiral, conical array, and mesh LCEAs were actuated on a hot plate held at 95 °C. Note, the spiral actuation was aided by a heat gun that was held above the actuator. All actuators were lubricated with silicone oil to prevent adhesion to the substrate prior to actuation.

Supporting Information

Supporting Information is available from the Wiley Online Library or from the author.

Acknowledgements

The authors gratefully acknowledge support from the National Science Foundation through the Harvard MRSEC (Grant No. DMR-1420570) and the DMREF (Grant No. DMR-1533985). A.K. and R.L.T. acknowledge support from their National Science Foundation Graduate Research Fellowships. J.A.L. acknowledges support from the Vannevar Bush Faculty Fellowship Program sponsored by the Basic Research Office of the Assistant Secretary of Defense for Research and Engineering and funded by the Office of Naval Research Grant N00014-16-1-2823 as well as the generous donation from the GETTYLAB in support of our work. This work made use of the Shared Experimental Facilities supported in part by the MRSEC Program of the National Science Foundation under award number DMR-1419807. Finally, the authors thank L. K. Sanders and C. Settens for technical assistance and Brian Donovan and Tyler Guin (AFRL) for useful discussions.

Conflict of Interest

Jennifer Lewis has co-founded a startup company, Voxel8, which focuses on multimaterial 3D printing.

Keywords

3D printing, actuators, liquid crystal elastomers, shape morphing

Received: October 23, 2017

Revised: November 19, 2017

Published online:

- [1] H. Wermter, H. Finkelmann, *e-Polym.* **2001**, *1*, 111.
 [2] D. L. Thomsen, P. Keller, J. Naciri, R. Pink, H. Jeon, D. Shenoy, B. R. Ratna, *Macromolecules* **2001**, *34*, 5868.
 [3] S. Palagi, A. G. Mark, S. Y. Reigh, K. Melde, T. Qiu, H. Zeng, C. Parmeggiani, D. Martella, A. Sanchez-Castillo, N. Kapernaum,

- F. Giesselmann, D. S. Wiersma, E. Lauga, P. Fischer, *Nat. Mater.* **2016**, *15*, 647.
 [4] M. Rogóž, H. Zeng, C. Xuan, D. S. Wiersma, P. Wasylczyk, *Adv. Opt. Mater.* **2016**, *4*, 1689.
 [5] M. K. McBride, M. Hendriks, D. Liu, B. T. Worrell, D. J. Broer, C. N. Bowman, *Adv. Mater.* **2017**, *29*, 1606509.
 [6] S. Schuhladen, F. Preller, R. Rix, S. Petsch, R. Zentel, H. Zappe, *Adv. Mater.* **2014**, *26*, 7247.
 [7] F. Greco, V. Domenici, A. Desii, E. Sinibaldi, B. Zupančič, B. Zalar, B. Mazzolai, V. Mattoli, *Soft Matter* **2013**, *9*, 11405.
 [8] T. H. Ware, J. S. Biggins, A. F. Shick, M. Warner, T. J. White, *Nat. Commun.* **2016**, *7*, 10781.
 [9] C. J. Camargo, H. Campanella, J. E. Marshall, N. Torras, K. Zinoviev, E. M. Terentjev, J. Esteve, *J. Micromech. Microeng.* **2012**, *22*, 75009.
 [10] J. Kupfer, H. Finkelmann, *Makromol. Chem., Rapid Commun.* **1991**, *12*, 717.
 [11] T. H. Ware, M. E. McConney, J. J. Wie, V. P. Tondiglia, T. J. White, *Science* **2015**, *347*, 982.
 [12] T. H. Ware, T. J. White, *Polym. Chem.* **2015**, *6*, 4835.
 [13] J. M. Boothby, H. Kim, T. H. Ware, *Sens. Actuators, B* **2017**, *240*, 511.
 [14] M. Yamada, M. Kondo, R. Miyasato, Y. Naka, J. Mamiya, M. Kinoshita, A. Shishido, Y. Yu, C. J. Barrett, T. Ikeda, *J. Mater. Chem.* **2009**, *19*, 60.
 [15] M. Yamada, M. Kondo, J. I. Mamiya, Y. Yu, M. Kinoshita, C. J. Barrett, T. Ikeda, *Angew. Chem., Int. Ed.* **2008**, *47*, 4986.
 [16] M. Camacho-Lopez, H. Finkelmann, P. Palffy-Muhoray, M. Shelley, *Nat. Mater.* **2004**, *3*, 307.
 [17] C. Yuan, D. Roach, C. Dunn, Q. Mu, X. Kuang, C. M. Yakacki, T. Wang, K. Yu, H. J. Qi, *Soft Matter* **2017**, *13*, 5558.
 [18] H. Yang, A. Buguin, J. M. Taulemesse, K. Kaneko, S. Méry, A. Bergeret, P. Keller, *J. Am. Chem. Soc.* **2009**, *131*, 15000.
 [19] C. H. Legge, F. J. Davis, G. R. Mitchell, *J. Phys. II* **1991**, *1*, 1253.
 [20] M. H. Li, P. Keller, J. Yang, P. A. Albouy, *Adv. Mater.* **2004**, *16*, 1922.
 [21] C. Ambulo, J. J. Burroughs, J. M. Boothby, H. Kim, M. R. Shankar, T. H. Ware, *ACS Appl. Mater. Interfaces* **2017**, *9*, 37332.
 [22] M. Wehner, R. L. Truby, D. J. Fitzgerald, B. Mosadegh, G. M. Whitesides, J. A. Lewis, R. J. Wood, *Nature* **2016**, *536*, 451.
 [23] I. A. Anderson, T. A. Gisby, T. G. McKay, B. M. O'Brien, E. P. Calius, *J. Appl. Phys.* **2012**, *112*, 41101.
 [24] T. J. White, D. J. Broer, *Nat. Mater.* **2015**, *14*, 1087.
 [25] C. Ohm, M. Brehmer, R. Zentel, *Adv. Mater.* **2010**, *22*, 3366.
 [26] J. W. Boley, K. Chaudhary, T. J. Ober, M. Khorasaninejad, W. T. Chen, E. Hanson, A. Kulkarni, J. Oh, J. Kim, L. K. Aagesen, A. Y. Zhu, F. Capasso, K. Thornton, P. V. Braun, J. A. Lewis, *Adv. Mater.* **2017**, *29*, 1604778.
 [27] A. R. Tajbakhsh, E. M. Terentjev, *Eur. Phys. J. E: Soft Matter Biol. Phys.* **2001**, *6*, 181.
 [28] P. Leduc, C. Haber, G. Bao, D. Wirtz, *Nature* **1999**, *399*, 564.
 [29] G. G. Viola, D. G. Baird, *J. Rheol.* **1986**, *30*, 601.
 [30] F. N. Cogswell, *Polym. Eng. Sci.* **1972**, *12*, 64.
 [31] C. Ohm, M. Morys, F. R. Forst, L. Braun, A. Eremin, C. Serra, R. Stannarius, R. Zentel, *Soft Matter* **2011**, *7*, 3730.
 [32] M. Warner, E. M. Terentjev, *Liquid Crystal Elastomers*, Oxford University Press, New York **2007**.
 [33] M. O. Saed, A. H. Torbati, C. A. Starr, R. Visvanathan, N. A. Clark, C. M. Yakacki, *J. Polym. Sci., Part B: Polym. Phys.* **2017**, *55*, 157.
 [34] A. S. Gladman, E. A. Matsumoto, R. G. Nuzzo, L. Mahadevan, J. A. Lewis, *Nat. Mater.* **2016**, *15*, 413.
 [35] M. Deutsch, *Phys. Rev. A* **1991**, *44*, 8264.